Measuring the Layer Thickness of MEMS by Measuring Torsional Resonance: Simulated Experiment

N. Andrews and J.V. Clark

Purdue University, West Lafayette, IN, USA, nandrews@purdue.edu and jvclark@purdue.edu

ABSTRACT

In this paper we propose a method for measuring the structural layer thickness of MEMS. Since layer thickness strongly influences MEMS behavior, the characterization of thickness can be used for quality control and to improve the control and prediction of MEMS performance. Typical methods for measuring layer thickness involve various optical techniques such as ellipsometry and interferometry, but such methods are not performance-based and not amenable for industrial-scale fabrication. Gupta first proposed a torsion structure for measuring layer thickness using a gap-closing actuator, computer simulation, and some assumptions about the values of material properties. Here, we improve Gupta's method by using comb drive levitation, analytical modeling, and eliminating material properties from the analysis. And we employ a simulated experiment to virtually validate our metrology method.

Keywords: layer thickness, electro micro metrology, EMM, torsional resonance, simulated experiment

1 INTRODUCTION

Structural thickness of planar MEMS can influence mechanical, thermal, and electrical behaviors. Measurement of layer thickness is often desired for calibration, quality control, and prediction of MEMS performance. In many cases the layer thickness can have squared, cubed, or higher power effects on MEMS performance.

There are several methods for measuring layer thickness [1]. Timing the deposition rate and estimating layer thickness provides a very easy but crude measurement which ignores process variation. Scanning electron microscopy (SEM) can provide good thickness measurements, but is time consuming, often requires sample preparation, and is usually destructive (for layer thickness measurement). Additionally, the alignment of viewing angle and the use of measurement bars while using SEM can be an ambiguous process which introduces human variation [1]. Stylus profilometry can be used to accurately measure steps and other geometrical structures, but has draw backs with released structures which can be deflected or damaged during the measurement [2]. Ellipsometry and interferometry are very mature fields and both methods are widely used. Ellipsometry is excellent for measuring continuous layers with suitable and known optical properties. A MEMS for measuring thickness that was presented in [7] uses a profilometer and an interferometer.

MEMS structures with changing geometries made of numerous non-standard materials (for optics, e.g. polymers or metals) require special treatment and effort. Some of the challenges faced are spot size, which can be larger than an entire MEMS structure, depolarization due to the different surface materials and structure, and the extensive modeling involved with the new materials used in MEMS [3]. Interferometry is similar to ellipsometry and also provides excellent accuracy and precision in certain circumstances, but suffers from some of the same challenges. Interferometry is more applicable for MEMS because of its use in measuring steps and trenches, but is still limited in deep trenches and other varying MEMS structures because of the varied optical effects of such structures [1], [2], [4]. Another interesting method for measuring layer thickness is micro-Raman spectroscopy where temperature change is used to back calculate the structure thickness during laser heating. Targeting of the structure can be very precise, but knowledge of material properties is needed and certain limitations on materials and structures apply [5].

Gupta appears to have proposed the first torsional resonator for measuring layer thickness [1]. The model is subject to squeezed-film damping, ignores warping, and assumes material properties. The advancement we make in the use of torsional resonance for measuring layer thickness is: elimination of squeezed-film damping, inclusion of warping, and elimination of unknown material properties.

The rest of this paper is organized as follows. In Section 2 we describe the design of our test structure. In Section 3 we describe our analytical and computer models. In Section 4 we perform a virtual experiment by using the analytical model to predict the layer thickness of the computer model. Last, we conclude with our findings.

2 TEST STRUCTURE DESIGN

We illustrate our proposed test structure in Figure 1. The device has a fixed-free 'T' shape, with a simple torsional comb drive at the free end. The structure is easy to fabricate and analyze. Because the design consists of a single device layer without ground electrodes, it can be fabricated with a single mask. Compared to the prior effort in [1], our design does not require multiple masks to create ground plane electrodes; it is not affected by squeezed-film damping, so it does not require vacuum sealing; and it is not affected by residual stress.

For measuring layer thickness, our approach is to compare the resonant frequencies of two such torsional resonators that differ only in flexure beam width. By

assuming that the two fabricated test structures share the same unknown material properties and overcut errors in geometry, we eliminate the extraneous unknowns and express the layer thickness as a function of a ratio of torsional resonant frequencies.

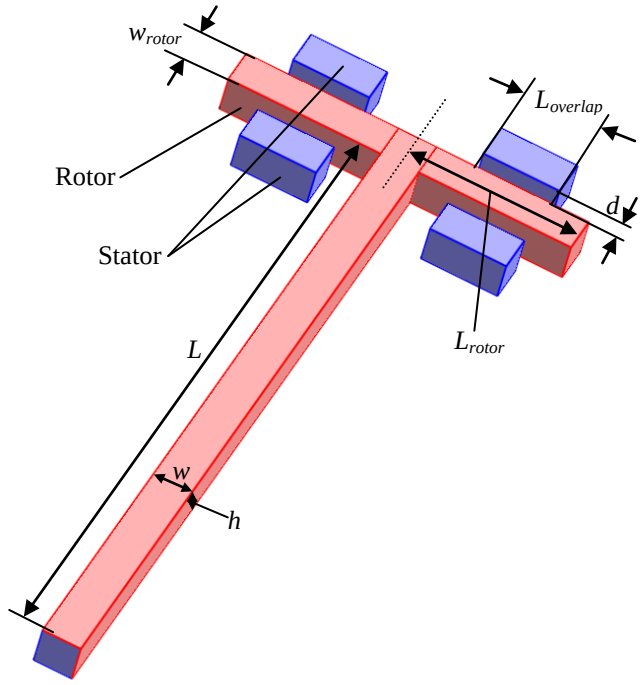

Fig. 1: Torsional resonator geometry. It operates by exciting a torsional resonant mode. Periodic comb drive levitation forces are applied 180 degrees out of phase to produce torsional excitation at the free end of the cantilever. Design parameters are identified. The stators and left end of the flexure are fixed.

To increase the chance of process variation consistency between both test structures (let's call the structures *a* and *b*), they should be fabricated within close proximity to each other. The fabricated torsional flexure widths ($w_a < w_b$) can be measured by our electrical probing technique [8]. The comb drive levitation effect, explained in [9], is used here to produce out-of-plane electrostatic forces. That is, due to the asymmetry about the comb drive fingers, there is a larger amount of surface charge on the top surface of the fingers than on the bottom surface of the fingers, which we exploit to produce torsional resonance. Because the width is different for each cantilever, their respective torsional resonant frequencies will differ, $\omega_{0,a} < \omega_{0,b}$. The parameters of our T-shaped design are given in Table 2.

3 MODELING

In this section we present a derivation of our analytical model that can be used to determine layer thickness given the measured resonance frequencies of two test structures. Our model derivation involves using the relationship between resonance frequency, stiffness, and moment of inertia. By taking the ratio of expressions for structures *a* and *b*, we eliminate the unknown material properties, which results in an expression where thickness is the only unknown.

Table 2: Nomenclature.

Parameter	Description
c	Couette flow damping
d	Comb drive gap distance
E	Young's Modulus
F	Comb drive levitation force
G	Shear Modulus
h	Layer thickness
I_m	Moment of inertia of test structure
$I_{flexure}$	Moment of inertia of torsion flexure
I_{rotor}	Moment of inertia of rotor finger
J	Polar second-area moment
J_{approx}	J not including warping
J_β	J including warping
k_φ	Torsional stiffness
L	Length of torsional flexure
L_{rotor}	Length of comb drive finger
$L_{overlap}$	Length of overlap between rotor and stator
w	Width of torsional flexure
w_{rotor}	Width of comb drive finger
α	Maximum function of ratio between h and w
β	Prandtl's stress function
μ	Viscosity of air
ν	Poisson's Ratio
ρ	Material density
ω_0	Torsional resonant frequency

3.1 Analytical model

The torsional resonant frequency of the test structure depicted in Fig. 1 is related to its torsional stiffness k_φ and moment of inertia I_m by

$$\omega_0 = \sqrt{k_\varphi / I_m}\ . \tag{1}$$

Torsional stiffness is defined as

$$k_\varphi \equiv JG / L\ , \tag{2}$$

where L is the length of the torsional flexure, and G is the shear modulus

$$G = \frac{E}{2(1+\nu)}, \tag{3}$$

where E is Young's modulus and ν is Poisson's ratio. If warping is not significant, the polar second-area moment J can be approximated by

$$J_{approx} = \frac{hw^3}{16}\left[\frac{16}{3} - 3.36\frac{w}{h}\left(1 - \frac{1}{12}\frac{w^4}{h^4}\right)\right], \tag{4}$$

for $h \geq w$. The h and w are switched if $w \geq h$ for all J. If warping is significant, J can be more accurately expressed in terms of the Prandtl's stress function $\beta(\alpha)$ [10]

$$J_\beta = \beta(\alpha) \times h w^3, \text{ for } h \geq w, \tag{5}$$

where

$$\alpha = \max\left(h/w,\ w/h\right) \tag{6}$$

is the maximum ratio between w and h of the torsional flexure. Prandtl's stress function is given as [10]

$$\beta(\alpha) = \frac{1}{3} - \frac{64}{\alpha \pi^5} \sum_{n=1,3,5,\ldots} \frac{1}{n^5} \tanh\left(\frac{\alpha n \pi}{2}\right). \tag{7}$$

In Fig. 2 we plot the relative error between J_{approx} and J_β, i.e. $(J_{approx} - J_\beta)/J_\beta$, as a function of $\alpha = h/w$. This plot is useful for determining which aspect ratio requires accurate modeling by (5) instead of being approximated by (4).

The moment of inertia I_m of the structure in Fig.1 can be decomposed into the moments of the torsional flexure and comb drive rotor as

$$I_m = I_{flexure} + I_{rotor}, \tag{8}$$

where the moment of inertia of the comb drive rotor is

$$I_{rotor} = \frac{1}{12} \rho h w_{rotor} \left(2L_{rotor}\right)\left(h^2 + \left(2L_{rotor}\right)^2\right), \tag{9}$$

and the moment of inertia of the flexure is [11]

$$I_{flexure} = \frac{1}{3} J \rho L. \tag{10}$$

Substituting these expressions into (1) we have

$$\omega_0^2 = \frac{JG}{\rho L}\left(\frac{1}{3} JL + \frac{h w_{rotor} \left(2L_{rotor}\right)\left(h^2 + \left(2L_{rotor}\right)^2\right)}{12}\right)^{-1}. \tag{11}$$

To eliminate unknown material properties (shear modulus and density) we take the ratio of the resonant frequencies of the two test structures a and b. For the case of accurate warping, we find:

$$\frac{\omega_{0,a}^2}{\omega_{0,b}^2} = \left(\frac{\beta_a {w_a}^3}{\beta_b {w_b}^3}\right)\left(\frac{\beta_b {w_b}^3 L + \frac{1}{4} w_{rotor} 2L_{rotor}\left(h^2 + \left(2L_{rotor}\right)^2\right)}{\beta_a {w_a}^3 L + \frac{1}{4} w_{rotor} 2L_{rotor}\left(h^2 + \left(2L_{rotor}\right)^2\right)}\right)$$

for $h \geq w_{a,b}$. If warping can be approximated, we have

$$\frac{\omega_{0,a}^2}{\omega_{0,b}^2} = \frac{\left(\frac{L}{3} + \frac{h w_{rotor}\left(2L_{rotor}\right)\left(h^2 + \left(2L_{rotor}\right)^2\right)}{4h w_b^3 - 2.52 w_b^4\left(1 - \frac{1}{12}\frac{w_b^4}{h^4}\right)}\right)}{\left(\frac{L}{3} + \frac{h w_{rotor}\left(2L_{rotor}\right)\left(h^2 + \left(2L_{rotor}\right)^2\right)}{4h w_a^3 - 2.52 w_a^4\left(1 - \frac{1}{12}\frac{w_a^4}{h^4}\right)}\right)} \tag{12}$$

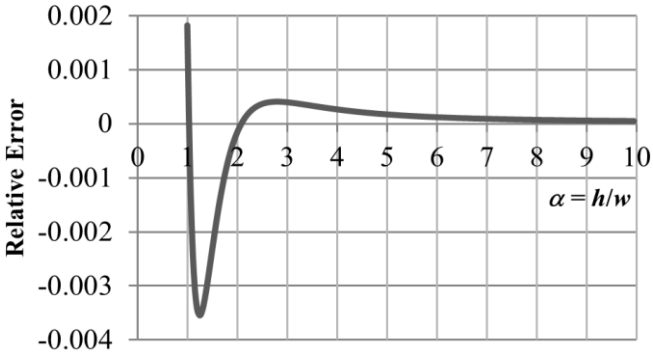

Fig. 2: Relative error between equations (4) and (5). The relative error when $h = w$ is 0.18%. The relative errors at the extrema are -0.36% and 0.041%. The relative error approaches 0 as the aspect ratio h/w becomes large.

for $h \geq w_{a,b}$. These expressions can be used to solve for the layer thickness h by using, say, a Netwon-Raphson method.

3.2 Finite Element Analysis

We use a finite element analysis (FEA) tool called COMSOL3.5a to compare and verify our analytical model. The torsional test structure was meshed with 90k tetrahedral elements (415k degrees of freedom) with fixed boundaries shown in blue in Fig. 1. The material properties were set to be isotropic poly silicon with a density ρ of 2300kg/m^3, a Young's modulus E of 165GPa, and Poisson's ratio v of 0.3. Fig. 3 shows the simulated mode 3 of the torsion flexure.

The electrostatic force due to the levitation effect was determined by simulating the surface charge density on the rotor as a function of voltage. Fig. 4 shows a cross section of the comb finger surrounded by the electric field. The rotor is located in the middle, with the two stators on either side. The rotor and bottom boundary are at potential V, the stators are grounded, and the outermost side and top boundaries are set to zero charge / symmetry. By integrating the electric Maxwell stress tenor of the top surface of the rotor and subtracting it from the bottom surface of the rotor, we find a net upwards vertical force on the rotor finger of

$$F = V^2 \times 6.74 \times 10^{-11}\ N \tag{13}$$

at the position shown in Fig. 4. With an applied periodic voltage of 20V, the levitation force is large enough to drive the structure into torsional resonance with an amplitude of about 1μm. We estimate the vertical amplitude with

$$y_{\max} = \frac{F}{c\omega_d} \approx \frac{F}{\left(\mu 2hL_{overlap}/d\right)\omega_0}. \tag{14}$$

3.3 Verification

We verify our analytical model by comparing it against our computer model. We performed convergence analysis on the computer model by refining the number of elements

until results became consistent (at $90k$ elements). Given identical geometric and material properties, our analytical and computer models yield torsional resonant frequency of $308.4kHz$ and $308.8kHz$, respectively. The relative error between them is 0.13%.

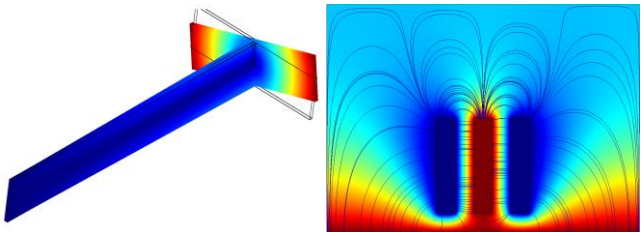

Fig. 3: FEA of torsional resonance and comb drive levitation. Eigen frequency of mode 3 is shown. Geometry is $h = 20\mu m$, $L = 200\mu m$, $w = 2\mu m$, and $L_{rotor} = 50\mu m$. The torsional resonant frequency is $308.8kHz$. A cross section of the comb drive is shown with electric field lines and voltage. Levitation force on the rotor is $F = V^2 \times 6.74 \times 10^{-11}\ N$.

4 VIRTUAL EXPERIMENT

We conduct a virtual experiment with our computer models. By virtual experiment, we mean that we only use simulation results that would be available in a real experiment. In this case we only use resonance frequency to determine layer thickness. It is assumed that width has already been measured by, say, our other electronically probed method [8]. Since we would not know material properties in a true experiment, we are able to prescribe arbitrary material properties within the computer model.

To perform the experiment, we configure two test structures with the same geometric overcut from layout and the same material properties. Recall, the only difference between the two structures is the original layout widths of the torsional flexure. E.g., if layout widths are 2.25 µm and 3.25 µm for *a* and *b*, then a 0.25 µm overcut would yield fabricated widths of 2 µm and 3 µm respectively. In the model we prescribe an 'unknown' layer thickness of $4\mu m$. The other dimensions of the beams are identical and listed as follows: $L = 200\mu m$, $w_{\text{rotor}} = 2\mu m$, $L_{\text{rotor}} = 2\mu m$. Using these values, the resonant frequencies of structures *a* and *b* are given as $\omega_{0,a} = 272.7101kHz$ and $\omega_{0,b} = 443.2804kHz$. By substituting these frequencies in (12), the layer thickness can be found iteratively. Using an initial guess for thickness of $5\mu m$ and iterating h to match the ratio of ${\omega_{0,a}}^2$ to ${\omega_{0,b}}^2$ with a tolerance of $O\left(10^{-3}\right)$, we find h to be $3.97\mu m$. This corresponds to an error of $0.03\mu m$, or relative error of 0.75%, for layer thickness.

5 CONCLUSION

We have presented a performance-based method for measuring layer thickness of fabricated MEMS using torsional resonance. The method requires measuring the resonance of two test structures. The simple 'T' shaped structures studied here are not unique. We compared our analytical model to computer model for a structure with good agreement. Our analytical model matched the FEA within 0.13%. To validate our method for measuring layer thickness, we conducted a 'virtual' experiment where FEA was used in place of a real device. Doing so allows us to validate our model against exactly known parameters, which is not possible to attain using a real device. Our 'virtual' experiment yielded good agreement with a relative error of 0.75%.

REFERENCES

[1] R. K. Gupta, "Electronically Probed Measurements of MEMS Geometries," *Journal of Microelectromechanical Systems*, Vol. 9, pp. 380-389, 2000.

[2] T. Guo, L. Ma, and Y. Bian, "MEMS Characterization Based on Optical Measuring Methods," *Microelectromechanical Systems and Devices*, N. Islam ed. Rijeka, Croatia: InTech, March, 2012, ch.5.

[3] M. Losurdo, M. Bergmair, G. Bruno, D. Cattelan, C. Cobet, A. de Martino, K. Fleischer, Z. Dohcevic-Mitrovic, N. Esser, M. Galliet, R. Gajic, D. Hemzal, K. Hingerl, J. Humlicek, R. Ossikovski, Z.V. Popovic, and O. Saxl, "Spectroscopic ellipsometry and polarimetry for materials and systems analysis at the nanometer scale: state-of-the-art, potential, and perspectives," *Journal of Nanoparticle Research*, Vol. 11, Iss. 7, pp. 1521–1554, 2009.

[4] J. Schmit and E. Novak, "Challenges in Interferometric Measurements of MEMS and Semiconductor Devices," *ASPE Proceedings*, Orlando, FL, 2004.

[5] X. Wu, J. Yu, T. Ren, and L. Liu, "Micro-Raman measurement of thickness in microelectromechanical silicon structures," *Journal of Micromechanics and Microengineering*, Vol. 17, Num. 6, pp. 1114-1120, 2007.

[6] P.M. Osterberg and S.D. Senturia, "M-TEST: A Test Chip for MEMS Material Property Measurement Using Electrostatically Actuated Test Structures," *Journal of Microelectromechanical Systems*, Vol. 6, Num. 2, pp. 107-118, 1997.

[7] J. C. Marshall, "New Optomechanical Techniques for Measuring Layer Thickness in MEMS Processes," *Journal of Microelectromechanical Systems*, Vol. 10, Num. 1, pp. 153-157, 2001.

[8] J. V. Clark, "Measuring Force, Stiffness, Displacement, and Geometry in the Face of Property Variation," *SEM2010 Annual Conference on Experiment and Applied Mechanics*, pp. 67-74, June 7-10, 2010.

[9] W. C. Tang, M. G. Lim, and R. T. Howe, "Electrostatic Comb Drive Levitation and Control Method," *Journal of Microelectromechanical Systems*, Vol. 1, pp. 170-178, 1992.

[10] Budynas, *Advanced Strength and Applied Stress Analysis*, 2nd ed., WCB/McGraw-Hill, 1999.

[11] Paz, *Structural dynamics: Theory and Computation*, 3rd ed., Van Nostrand Rein, 1991.

[12] Ghali, *Structural Analysis: A Unified Classical and Matrix Approach*, A.M. Neville 4th Ed., E & FN Spon, 1997.